Voltage-Sensitivity-Approach-Based Adaptive Droop Control Strategy of Hybrid STATCOM

Sungyoon Song, *Student Member, IEEE*, Changhee Han, *Student Member, IEEE*, Gyu-Sub Lee, *Member, IEEE*, Roy A. McCann, *Senior Member, IEEE*, and Gilsoo Jang, *Senior Member, IEEE*

***Abstract*—In this study, we propose an adaptive droop control strategy for application to hybrid static synchronous compensator (STATCOM) systems. The proposed voltage-sensitivity-based adaptive droop control scheme using a hybrid STATCOM system helps eliminate any possible interference from other voltage regulation devices while achieving better voltage regulation without implementation of a full observation of the corresponding network. Sensitivity analysis was performed by voltage control of the STATCOM system, and sliding-mode control was included for robustness of the control system. The fixed and adaptive control methods were compared through case studies of the IEEE 39-bus test system. The results were further verified through a transient simulation of the hybrid STATCOM system by considering both low- and high-penetration levels of inverter-based resources.**

***Index Terms*—Adaptive droop control, hybrid STATCOM, sensitivity analysis, voltage regulation.**

I. Introduction

THE considerable increase in distributed generations (DGs), especially based on inverter-based resources (IBRs), is expected to provide advantages such as greenhouse gas emission reduction, energy sustainability, and energy security [1]. However, because of the intermittency of IBRs, revolutionary changes in grid planning and operation are required [2], [3]. Frequency events occur in tandem with voltage events, and the uncertain response of IBRs to low voltage events contributes to the uncertainty of grid frequency responses. Thus, voltage regulation for multiple reactive power resources connected to AC networks has become more important nowadays [4].

Traditionally, voltage was regulated in operational boundaries using additional facilities such as on-load tap changers (OLTCs), step voltage regulators (SVRs), and capacitor banks (CBs). However, the tap adjustment of the OLTC and SVR and the switching of the CB are limited because of their slow responses and discrete characteristics [5]; therefore, addressing the voltage violation in real-time with high accuracy is a difficult task. To overcome these limitations, high-voltage, high-current power electronic devices such as static synchronous compensator (STATCOM) are adopted to maintain a stable voltage. However, because the use of the STATCOM frequently leads to concerns regarding cost efficiency for system operators, the concept of hybrid STATCOM systems has been introduced to reduce the large initial capital outlay. A small portion of the total capacity of such a system is obtained from the STATCOM, and the remaining is obtained from other reactive power resources (e.g., CB, SVR) [6].

Furthermore, DGs have also been recently exploited for voltage regulation. Specifically, to address this issue, the recent IEEE standard, IEEE 1547, considers the capability of the DG to support voltage regulation [7]. In [7], DGs provided the capabilities of four reactive power supporting modes: power factor mode; voltage-reactive power mode; active power-power factor mode; and reactive power mode. To achieve these control capabilities, advanced features of power electronic interfaces for reactive power support are required, and the concept of smart inverters was widely adopted for various studies [8], [9].

To coordinate various voltage regulation devices, methods to manage reactive power resources have been introduced by previous studies. Control strategies ranging from centralized to completely decentralized were proposed to address these challenges. Researchers first focused on centralized approaches, which means that all data are gathered at a single point, where a central processor makes control decisions [10], [11]. Model-based methods have been generally applied for better voltage management of multiple reactive power resources. However, the complex nonlinearities of power and voltage in the optimal power flow model make it time consuming to solve the problem [12]–[14]. In addition, these approaches require parameters and operation points to be updated every time the state of the network changes because the resulting output obtained for a given period will not necessarily be valid for the next one because of the inherent changes in the load and generation. Thus, all reactive power resources must communicate with all other resources or a central controller, thus requiring network observability and a dense communication architecture.

To eliminate the need of remote monitoring, decentralized droop control strategies [15], [16] or surface fitting techniques [17] have been proposed. However, accuracy can be compromised, particularly when new resources are connected to the

Manuscript received January 28, 2020; revised April 6, 2020 and May 22, 2020; accepted June 8, 2020. Date of publication June 19, 2020; date of current version January 6, 2021. This work was supported in part by the National Research Foundation under Grant 2017K1A4A3013579 and in part by the Ministry of Trade, Industry & Energy, Republic of Korea, under Grant 20174030201540. Paper no. TPWRS-00139-2020. *(Corresponding author: Gilsoo Jang.)*

Sungyoon Song, Changhee Han, and Gilsoo Jang are with the School of Electrical Engineering, Korea University, Seongbok-gu 02841, South Korea (e-mail: blue6947@korea.ac.kr; hch0806@korea.ac.kr; gjang@korea.ac.kr).

Gyu-Sub Lee is with the School of Electrical Engineering, Seoul National University, Seoul 08826, South Korea (e-mail: lgs1106@snu.ac.kr).

Roy A. McCann is with the School of Electrical Engineering, Arkansas University, Fayetteville, AR, 72701 USA (e-mail: rmccann@uark.edu).

Color versions of one or more of the figures in this article are available online at https://ieeexplore.ieee.org.

Digital Object Identifier 10.1109/TPWRS.2020.3003582

network because the current standard is to employ proportional control loops locally at each inverter. The timetable or three-dimensional fitting curves should also be updated to prepare for network topology changes. Adopting coordinated time delays on every reactive power resource [5], [18], [19] is impractical for bulk power systems because time delay settings should be kept updated. The published literature has a significant disadvantage in that the sensitivity must be recalculated and direct voltage regulation with inaccurate sensitivity may interfere with other voltage regulation devices, it is prohibited by IEEE 1547.

The intelligent voltage regulation strategies of DGs have also been addressed in distribution networks and have subsequently been aggregated into a hierarchical control architecture [16]. In [20], an algorithm for the optimal voltage regulation of distribution secondary networks with DGs was proposed, and a remote-terminal-unit-based method using DGs for voltage control in a distribution network was proposed in [21]. In [22], a method to prevent voltage from exceeding the upper operating limit was proposed by changing the reactive power generation of a DG. [23] and [24] not only presented a voltage control method with an energy storage system but also offered a method for coordinating DGs and smart inverter devices to minimize the absolute voltage magnitude deviation via a linear program.

All these references mostly discuss how DGs can regulate voltage by adjusting their generations. However, the system operator cannot regulate the sitting and parameters of DGs that renewable energy providers possess. The inverter-interfaced DGs are mostly driven by variable-output IBRs such as photovoltaic system and for this reason are considered as non-dispatchable and uncontrollable. They participate in voltage regulation to the minimum to satisfy grid code. In addition, voltage stability can be compromised if the STATCOMs adjust their output voltage in an attempt to restore the grid without any feedback from other resources while operating autonomously.

In this study, therefore, a novel adaptive droop control logic based on the voltage-sensitivity-approach for hybrid STATCOM is introduced with frequent network topology changes, especially under the uncertain penetration of IBRs. Our designs overcome the limitations of existing strategies by combining the decentralized droop control and sliding-mode control with adaptive droop and not the fixed droop gain. Therefore, it is an attractive interim option before implementing more complex schemes. In summary, the main contributions of this paper are as follows:

- The architecture allows flexibility and redundancy even with unforeseen network topology change without implementing full observation of the corresponding network.
- We eliminate the possibility of interference with the other uncontrollable voltage regulation devices by locally adjusting STATCOM reactive power.
- More precise voltage control is possible by providing localized information in primary control.
- STATCOM can prepare for *N*-1-1 contingency and immediate IBR output power, thereby achieve better total voltage regulation with CB.

The rest of the document is structured as follows. The problem is formulated in Section II and Section III explains the

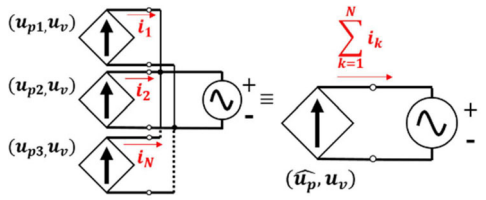

Fig. 1. Aggregated IBR model with the same model structure as an individual inverter.

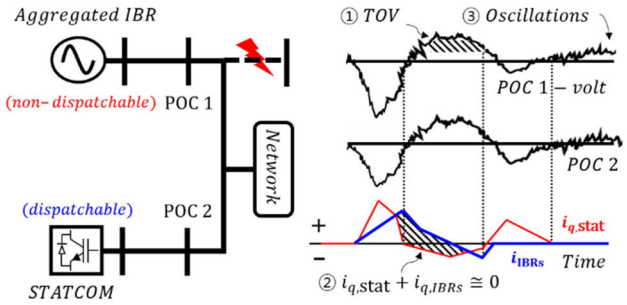

Fig. 2. Degraded control actions between reactive power resources.

general hybrid STATCOM model. Sections IV and V deal with the sliding-mode-control-based adaptive control strategy and operation strategy. In Section VI, simulation studies have been performed on the IEEE 39-bus standard test system.

II. Problem Formulation

In this section, we clearly demonstrate the fundamental limitation of voltage control under uncontrollable IBRs. The presentation frames and motivates our subsequent controller designs. For simplicity, the IBRs are designed by the equivalent model based on aggregated modeling [25], [26], and the model follows a reduced-order aggregated model for *N* parallel-connected IBRs as shown in Fig. 1. A complete survey of the equivalent model is beyond the scope of this study; we have provided a short summary here.

The dynamics of a multi-IBR system can be modeled exactly as one aggregated equivalent inverter model when the control and physical parameters of each IBR adhere to a set of scaling laws as follows:

$$\mu_{px} : \frac{p_{rated}}{p_{base}}, \quad \mu_v : \frac{v_{rated}}{v_{base}}. \tag{1}$$

where u_{px} and u_p are the power and voltage scaling factors, respectively, and p_{base} and v_{base} are system-side based values. For example, IBR 1, 2, and 3 have power ratings of approximately 1 MW, 1 MW, and 0.5 MW, respectively, and we arbitrarily pick the power base value as $p_{base} = 1$ MW. This implies power scaling factors of $u_{p1} = 1$, $u_{p2} = 1$, and $u_{p3} = 0.5$ for the multi-inverter system, and $\widehat{u_p} = 2.5$ for the aggregated equivalent IBRs. See [26] for a detailed modeling procedure.

STATCOM is represented by a voltage source converter (VSC) model and modeling procedure of STATCOM system is illustrated in Section III. As shown in Fig. 2, a drop in voltage

at the point of coupling (POC) 1 because of an arbitrary fault or immediate IBR output power leads to a simultaneous drop in the voltage at POC 2 when the two points are electrically close. In this case, both IBR and STATCOM generate reactive currents ($i_{q,IBRs}, i_{q,stat}$) into the grid under their own control schemes and control parameters. The dynamics of IBR is slower than STATCOM as shown by the blue trace in Fig. 2 because IBRs will be involved in voltage regulation to a minimum only to satisfy the grid code. It is noteworthy that synchronous generators or OLTCs with slow dynamics are not considered in this issue.

As expected, two reactive power resources instantaneously generate reactive power based on the sudden voltage drops, as shown in Fig. 2 and degraded dynamic control action can be observed as follows: 1) If a large amount of IBR is concurrently connected with the power system under the peak load condition, the voltage is consistently maintained because several reactive power resources are present and are actively used.

Nevertheless, STATCOM unnecessarily generates a large amount of reactive power based on the instantaneous voltage drops, which reduces the capability to prepare for the *N*-1-1 contingency. Furthermore, the sum of the two reactive power outputs is often zero right after a fault, as shown in Fig. 2. 2) If a small number of IBR is connected with the grid in the off-peak load condition, voltage easily becomes unstable when a fault occurs. Thus, it is appropriate to change a droop gain for better voltage regulation. Degraded control interaction between STATCOM and other inverter-based reactive power resources occurs owing to the lack of accurate knowledge regarding the placement or unadjusted parameters. And, these issues can also be caused by immediate IBR power output. Consequently, this phenomenon induces several disadvantages as follows:

1) Temporary over-voltage conditions at the respective POC immediately after a fault.
2) Unstable voltage profile at the respective POC after a fault.
3) Degraded control interaction and oscillations between the reactive power resources.
4) Reduction of the capability of the reactive power resource to cope with an *N*-1-1 contingency.
5) Requirement of individual control after a fault.

Thus, the control objective is to mitigate the above issues using the hybrid STATCOM system. A detailed description is provided here.

III. Hybrid STATCOM Model Configuration

In this phase, the hybrid STATCOM system, which is a combination of STATCOM and CBs, is introduced, as shown in Fig. 3. A similar system is present at the San Diego Gas & Electric system for dynamic Var control during peak load conditions [27]. This system control maintains the output of the reactive power to a minimum value, and if the reactive power from STATCOM is outside a dead band for a specified time, a control signal connects or disconnects the CBs. As another project, the Holly STATCOM in Austin, Texas, which is based on the SVC Light platform of ASEA Brown Boveri (ABB), is combined with two types of 31.2 Mvar CBs. It utilizes the

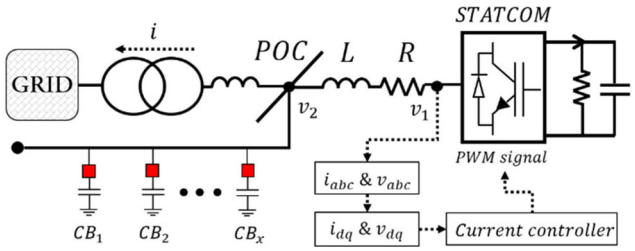

Fig. 3. Simplified diagram of hybrid STATCOM system.

MACH2 control system, a common control platform used for all ABB FACTS and HVDC Projects [28].

The modeling procedure for the hybrid STATCOM is similar to the approach used in [29], [30], which is described here briefly. The basic proof of concept of the STATCOM has already been demonstrated through hardware experimentation with the developed prototypes [30], [31]. The previous works related to designing a robust damping controller also demonstrate an effective performance for a range of operating conditions of the nonlinear power system [32].

For modeling of the controller, the widely used vector control is applied. Its function is to act as a fully controllable voltage source, matching the phase and frequency of the system voltage, with an amplitude that can be continuously controlled. Let the STATCOM side impedance be simply modeled as a series-connected three-phase impedance. Furthermore, let the reference voltage generated by the inner current control loop be transformed back into the abc frame and used for pulse with modulation (PWM) to produce the desired converter three-phase voltage.

$$\begin{bmatrix} v_1^d \\ v_1^q \end{bmatrix} - \begin{bmatrix} v_2^d \\ v_2^q \end{bmatrix} = R \begin{bmatrix} i_d \\ i_q \end{bmatrix} + L \frac{d}{dt} \begin{bmatrix} i_d \\ i_q \end{bmatrix} - \begin{bmatrix} -\omega L i_q \\ \omega L i_d \end{bmatrix}, \quad (2)$$

where v_2 is the voltage at POC and v_1 is the voltage at the converter. In addition, R and L are the resistance and inductance, respectively, and i is the current flowing to the AC grid, as shown in Fig. 3. The reference voltage generated by the inner current control loop is transformed back into the abc frame and PWM to produce the desired converter three-phase voltage. The voltage reference sent to the PWM is represented as follows:

$$\begin{bmatrix} \Delta v_2^d \\ \Delta v_2^q \end{bmatrix} = - \begin{bmatrix} A_d(s) \\ A_q(s) \end{bmatrix} \begin{bmatrix} \Delta i_{d,ref} - \Delta i_d \\ \Delta i_{q,ref} - \Delta i_q \end{bmatrix} + \omega L \begin{bmatrix} -\Delta i_q \\ \Delta i_d \end{bmatrix} + \begin{bmatrix} v_1^d \\ v_1^q \end{bmatrix}, \quad (3)$$

where $A_d(s)$ and $A_q(s) = \frac{k_p s + k_i}{s}$.

The instantaneous powers at the AC and DC sides are equal assuming no losses, and the q-axis current of the d-q frame is aligned with the AC system phasor based on a phased-locked loop (PLL), i.e., $v_q = 0$. Therefore, DC voltage control, AC voltage control, and droop control can be all achieved using

$$P = 3/2 \left(v_d i_d \right), \quad (4)$$

$$Q = -3/2 \left(v_d i_q \right). \quad (5)$$

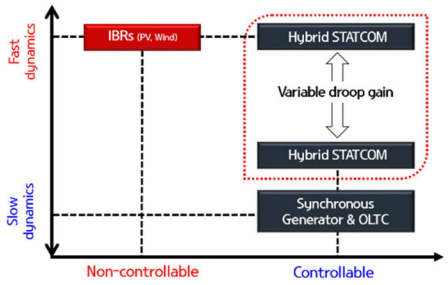

Fig. 4. Final control object of hybrid STATCOM.

In general, the CBs were combined with a STATCOM in the hybrid STATCOM system, as shown in Fig. 3. The dynamics of the CBs that are related to connection and disconnection requires some response delay time because of the mechanical characteristics, and it is not possible to switch it on again immediately unless the capacitor is discharged. The reactive power of a group of CBs decreases with the square of the POC voltage, as shown in (6) and (7):

$$Q_{CBs} = \sum_{\forall x \in l} Q_{CB,x}, \tag{6}$$

$$Q_{CB,x} = b_{CB,x} \times U_{poc}^2, \tag{7}$$

where $Q_{CB,x}$ refers to the total output reactive power at the x^{th} CB and l is the maximum number of installed CB devices. $b_{CB,x}$ is the susceptance of x^{th} CB. CBs are limited by the slow response and discrete voltage regulation, unlike the STATCOM system. By combining with the proposed operation strategy, the dynamic support range of hybrid STATCOM could be more improved than the only STATCOM system, and this combination provides better capability to voltage regulation.

IV. Proposed Adaptive Droop Control Strategy

A. STATCOM-Control-Based Voltage Sensitivity Analysis

This section introduces a general and fully distributed framework for novel adaptive droop control and voltage control. The control concept for adaptive droop control is based on the Q–V sensitivity analysis by STATCOM voltage control. In addition, the control object is to change the Q–V droop gain according to the results of the sensitivity analysis, as shown in Fig. 4. The flexible STATCOM control acts as a buffer, and it facilitates solving several issues described in Section II.

In the centralized method, at each operating point, the sensitivity of reactive power output to deviations in voltage is obtained by $\Delta V = \mathrm{J}_R^{-1}\Delta Q$. J_R^{-1} is the computing the power flow Jacobian, linearizing the power flow equations regarding the operating point [33]. Q–V Jacobian should be updated each time based on the state of the network changes. we may keep P constant and evaluate the voltage stability by considering the incremental relationship between Q and V. Note, the effects of changes in the system load or power transfer level are considered by studying the incremental relationship between Q and V at different operating conditions. Therefore, it requires the sensitivities to be updated every time the state of the network changes by EMS.

In this study, however, $\partial Q/\partial V$ is calculated by STATCOM control to estimate sensitivity without further monitoring and without any communication infrastructures. The sensitivity analysis is performed using the following expression:

$$\frac{\Delta \boldsymbol{Q}}{\Delta s \boldsymbol{V}} = \frac{\partial Q_j}{\partial v_j} = \frac{Q_j - Q_{j,0}}{v_j - v_{j,0}}, \quad j \in M. \tag{8}$$

Variation in reactive power output is measured when the voltage controller changes its set reference point at j^{th} STATCOM. Thus, $Q_{j,0}$ and $v_{j,0}$ are updated in 1- or 5-min intervals and Q_j and v_j are changed in real-time. The absolute value of sensitivity differs when employing the centralized and decentralized methods. However, the overall trend is similar under the various operating point. It is assumed that there are a total of *M* hybrid STATCOMs, where the j^{th} STATCOM takes the proposed adaptive droop control scheme, and each STATCOM has its own Q–V sensitivity of respective POC. Here, $(Q_{j,0}, v_{j,0})$ corresponds to the STATCOM operating conditions, and ∂Q_j is the deviation of the reactive power from its nominal value at the j^{th} STATCOM. The initial value of $\partial Q_j/\partial v_j$ is the instantaneous sensitivity just after the voltage reference change occurs at the j^{th} STATCOM, before any other controls become active.

For simplicity of exposition, an increased number of reactive power resources results in a high $\partial Q/\partial v$ because multiple resources located next to the STATCOM hold their bus voltages, and they can share the burden of voltage variations. Hence, a large reactive current should be generated on the STATCOM side if a change occurs in the voltage reference. In contrast, a decrease in the penetration level of reactive power resources will result in a low $\partial Q/\partial v$. For a lower overall $\partial Q/\partial v$, the STATCOM location should be electrically further away from a stiff reactive power source, such as a group of IBRs. If a group of reactive power resources is located further away from the STATCOM, there is lesser burden on STATCOM in the event of a voltage reference change because the reactive power resources require less reactive power. In general, the following approximation is valid without the introduction of considerable error:

1) The stiffness of the j^{th} STATCOM bus depends on the level of a group of nearby reactive power resources and the correlation is positive.
2) $\partial Q_j/\partial v_j$ shows the scaled samples of stiffness of the j^{th} STATCOM bus.
3) The penetration level of IBRs located close to the j^{th} bus can be estimated because the penetration level and $\partial Q_j/\partial v_j$ are proportional.

By obtaining the sensitivity result $(\partial Q/\partial v)$, the STATCOM changes the droop gain. Tuning the STATCOM voltage controller off provides a simple and intuitive trade-off between the conflicting goals of precise voltage regulation and uncontrollable IBRs with voltage regulation. For example, the STATCOM can recognize whether there are IBRs which has a voltage regulation capability. In other words, if at any time, due to any system network topology change, the sensitivity result changes, the droop gain of STATCOM is switched to the preset value in the economic dispatch cycle. This is called adaptive droop control

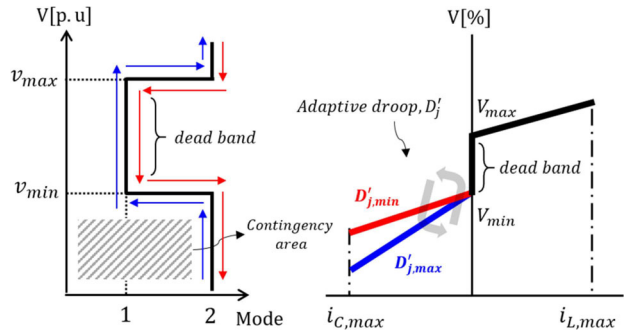

Fig. 5. Proposed adaptive droop characteristic of hybrid STATCOM system.

TABLE I
THE CONTROL OBJECT IN MODE 1 AND 2

Mode 1 (S=1)	Mode 2 (S=0)
• Voltage control at 1- or 5min intervals	• Sliding-mode-control-based droop control
• Estimate network topology changes • Steady-state condition	• Prepare a contingency • Dynamic condition

strategy. In general, decentralized droop controllers force the bus voltages to deviate from their nominal values in primary control [34] because the current standard is to employ proportional control loops locally at each inverter. Thus, several issues arise, as described in Section II. The proposed strategy provides an attractive advantage that more precise voltage control is possible by providing localized information in primary control. The detail control structure is illustrated in the next section.

B. Adaptive Droop Control of Hybrid STATCOM

As shown in Fig. 5, the proposed adaptive control for STATCOM includes the following two parts: 1) Mode-1: voltage control for sensitivity analysis, and 2) Mode-2: sliding-mode-control-based adaptive droop control.

$$\text{Mode 1}: v_{j,ref}(t) = S \times \left[v_{j,0} \pm v_{j,ch}\ (t + t_{j,st})\right], \tag{9}$$

$$\text{Mode 2}: Q_{j,ref}(t) = S \times \left[Q_{j,0} + \left(\frac{v_{j,ref} - v_{j,mes}(t)}{D'_j}\right)\right]. \tag{10}$$

where $v_{j,ref}$ refers to the nominal voltage reference at the j^{th} STATCOM, and $v_{j,mes}$ is the measured voltage at POC. $v_{j,0}$ and $Q_{j,0}$ are the initial voltage and reactive power, respectively. $D_{j,0}$ is the nominal droop value; thus, $D'_j = D_{j,0}$ in an initial state. $t_{j,st}$ is the time interval, which depends on the online economic dispatch cycle.

In general, the system operator uses a 1- or 5-min central dispatch cycle of generation; thus, it is suitable to set the $t_{j,st}$ value to a 1- or 5-min cycle, thereby activating mode-1 in that interval, as described in Table I. Note that $\partial Q/\partial v$ is predominantly affected by a stiff voltage resource; $t_{j,st}$ should be larger than the economic dispatch cycle, because changes network topology may significantly affect voltage sensitivity. Furthermore, mode-1 only works within the defined dead band as shown in Fig. 5 and the STATCOM is continuously modified by the addition or subtraction of an additional voltage reference such as $v_{j,ch}$ to measure the $\partial Q/\partial v$. On the other hand, operation in mode-2 is only possible without the dead band because droop control is implemented in case of contingency.

In addition, the $v_{j,0} \pm v_{j,ch}$ term should not violate a system reliability standard; the term should have a specific dead band as follows:

$$\begin{aligned} v_{min} - v_{j,0} &< v_{j,ch} < v_{max} - v_{j,0} \quad \text{or} \\ -v_{min} + v_{j,0} &> v_{j,ch} > -v_{max} + v_{j,0}\,. \end{aligned} \tag{11}$$

To transition between the two control modes, S and Not Gate are introduced and separate modes 1 and 2 as follows:

$$S = \begin{cases} 0, \ if \ \ v_{min} > v_{j,mes}(t) \ \ or \ v_{j,mes}(t) > v_{max}, & (12) \\ 1, \ if \ \ v_{min} \le v_{j,mes}(t) \le v_{max}, & (13) \end{cases}$$

By adopting (12)–(13), if the measured voltage represented as $v_{j,mes}$ is smaller than the v_{min} that represents the minimum allowable voltage at POC, the j^{th} STATCOM recognizes the presence of a fault. That is, if at any time, owing to any system disturbance, the POC voltage violates the allowable bounds, the binary signal S is switched to 0, as shown in Fig. 6. If the voltage is successfully regulated to within the utility specified range, mode-1 is performed again to estimate the levels of the nearby reactive power resources. Using the sensitively results from (8), the droop value is adaptively changed thorough the four parts, as follows:

$$D'_j = \begin{cases} D_{j,0}, \\ if\ Q_{j,1/2} - \varepsilon \le \partial Q_j/\partial v_j \ \le Q_{j,1/2} + \varepsilon, & (14) \\ D_{j,min}, \\ if\ \partial Q_{j,min}/\partial v_j < \partial Q_j/\partial v_j \ < Q_{j,1/2} - \varepsilon, & (15) \\ D_{j,max}, \\ if\ Q_{j,1/2} + \varepsilon < \partial Q_j/\partial v_j \ < \partial Q_{j,max}/\partial v_j, & (16) \\ D_{j,min}. \\ if\ v_{j,mes} < v_{min}. & (17) \end{cases}$$

where $Q_{j,1/2} = (\partial Q_{j,min}/\partial v_j + \partial Q_{j,max}/\partial v_j)/2$.

Here, $\partial Q_{j,min}/\partial v_j$ and $\partial Q_{j,max}/\partial v_j$ are calculated by $v_{j,ref} = v_{min}$ and $v_{j,ref} = v_{max}$ at mode-1 in the offline state. ε is the user-defined positive sensitivity and $D_{j,min}$ and $D_{j,max}$ are the minimum and maximum droop values, respectively. By observing (14), we note that the measurement variable $\partial Q_j/\partial v_j$ remains a small dead band. This implies that there is little change in the network topology near the j^{th} STATCOM; thus, only the nominal droop $D_{j,0}$ was used. If the network topology is changed, both (15) and (16) are applied to modify the droop gain. If the $\partial Q_j/\partial v_j$ is located within the range of (15), it can be assumed that few reactive power resources are connected near the j^{th} STATCOM bus. In contrast, if $\partial Q_j/\partial v_j$ belongs to the range of (16), it can be assumed that there are a large number of reactive power resources that actively participate in voltage regulation. A simple example involving equations (14)–(16) is illustrated by green box in Fig. 6. Lastly, a STATCOM must be able to provide maximum dynamic support during a fault; thus, D'_j should be updated by $D_{j,min}$ based on (17). Even if contingency to occur before the droop gain changes, the proposed strategy can cope with serious contingency by (17).

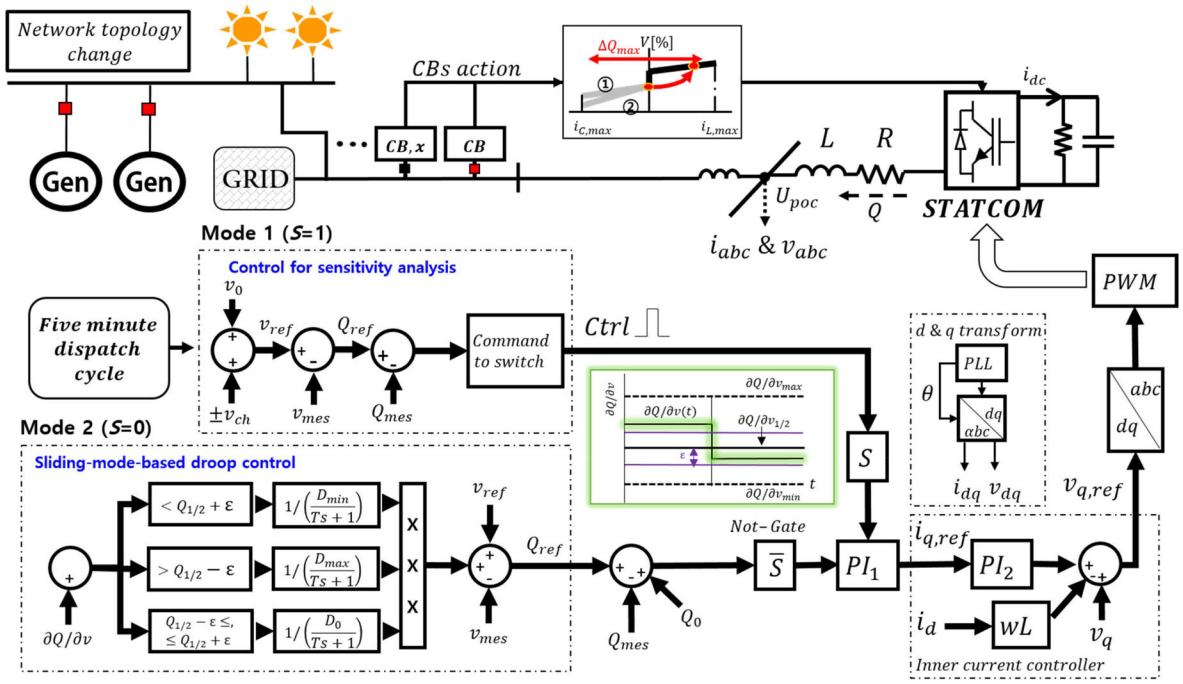

Fig. 6. Proposed sliding-control-mode-based adaptive droop control of hybrid STATCOM.

Although the droop gain can be determined further, specifically, frequent changes of droop gain are not desirable for converter stability [35]; thus, three kinds of droop gains were applied in this study.

V. Design and Operation Strategy of Adaptive Droop Control

A. Design of Adaptive Droop Controller

D_{min} should not drop to D_{max} immediately but must decrease exponentially due to the low pass filler. At the same time, D_{max} should not be changed immediately to D_{min}. Thus, the first order filter is applied. Assuming the $\varepsilon = 0$ for clarity, the control loops for D_{min} and D_{max} can be written as follows:

$$D'_j = D_{j,0} + (D_{j,max} - D_{j,0}) \cdot \frac{1}{1+sT}, \mathrm{Q} > Q'_{1/2}, \quad (18)$$

$$D'_j = D_{j,0} + (D_{j,min} - D_{j,0}) \cdot \frac{1}{1+sT}, \ \mathrm{Q} \le Q'_{1/2}. \quad (19)$$

Where, $Q'_{1/2}$is reactive power output when calculating sensitivity $Q_{1/2}$. Using voltage-sensitivity results, D'_j can be changed to $D_{j,max}$ or $D_{j,min}$ in the 1- or 5- min intervals. The small value of T ensures rapid increase or decrease in D'_j for effective prevention of large and uncertain voltage fluctuations. Additionally, it can reduce low-frequency oscillations owing to improved phase delay.

Combining (14)–(19), a bang-bang control loop is formed. To obtain a stable adaptive droop scheme, sliding mode control, which is a robust method to control nonlinear and uncertain systems, is proposed in this paper. The state-feedback control law is not a continuous function of time. Instead, it can switch from one continuous structure to another based on the current position in the state space. Hence, sliding mode control is a variable structure control method. The convergence of the droop gains and reactive power to the limiting value can be explained with the sliding-mode control theory. The control object is system stabilization in the presence of disturbances of droop gain change, as follows:

$$\lim_{t\to\infty} D'_j(t) - D_{j,max} = 0, \quad \lim_{t\to\infty} D'_j(t) - D_{j,min} = 0 \quad (20)$$

Thus, the control design approach consists of two steps. 1) A sliding manifold is designed such that the system trajectory along the manifold acquires certain desired properties. Therefore, the droop range of $0 < D_{min} < D_{j,0} < D_{max}$ is defined. 2) Discontinuous control is designed such that the system trajectories reach the manifold in finite time, as shown in (14) to (19).

As mentioned, there may be chattering and oscillation around the switching surface due to the variable structure control. For bounded disturbances and uncertainties, the Lyapunov function should still move toward zero [15]. Thus, convergence analysis was performed based on the definition of control law of $\dot{s}(x) \cdot ss(x) < 0$. Defining variable $x = 1/Q$ and combining $Q = \frac{v_{ref} - v_{mes}}{D} + Q_0$, we have

$$x = \mathbf{A} \cdot D' + \mathbf{B} = \frac{1}{v_{ref} - v_{mes}} \cdot D + Q_0. \quad (21)$$

Note that v_{mes} is considered as a time-invariant value because v_{mes} is measured in the steady-state at the operating point of $t = t + t_{j,st}$. In addition, the state-space equation can be written as $\dot{x} = A \cdot \dot{D'}$. Considering $D_{j,0}$ is constant for linearization, the input signal u can be written as $T \cdot \dot{D'} + D_0 = u$. Then, the u

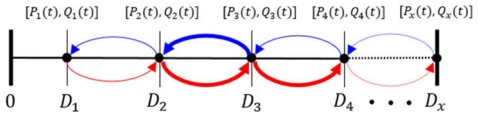

Fig. 7. Possible paths of droop gain in sliding-mode-control.

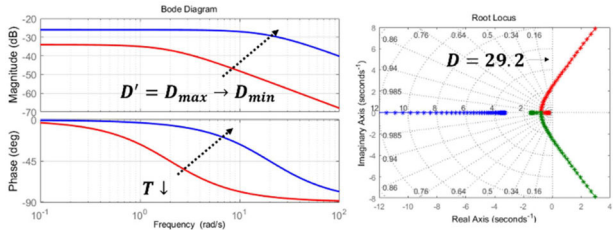

Fig. 8. (a) Bode plot of bang-bang control with varying $D'(0.02, 0.05\text{pu})$ and $T(0.1\ s, 0.01\ s)$. (b) Paths of dominant eigenvalues with droop gain increase

is defined in the control law as follows:

$$\begin{cases} u = D_{j,min}, & s(x) > 0, \\ u = D_{j,max}, & s(x) \le 0. \end{cases} \tag{22}$$

Thus, switching surface $s(x)$ is given by $s(x) = x - 1/Q'_{1/2}$ and the state-space equation can be written as follows:

$$\dot{x} = f(x) + g(x)\, u = \frac{A \cdot (-D_{j,0} + u)}{T}, \tag{23}$$

Therefore, the product of $s(x)$ and its derivative is given by

$$\dot{s}(x) \cdot s(x) = \dot{x} \cdot s(x) = \frac{A}{T} \cdot (-D_{j,0} + u) \cdot s(x), \tag{24}$$

$$\begin{cases} \dot{x}_1(x) = A/T \cdot (-D_{j,0} + D_{j,min}) \\ \dot{x}_2(x) = A/T \cdot (-D_{j,0} + D_{j,max}) \end{cases}. \tag{25}$$

Considering the $0 < D_{j,min} < D_{j,0} < D_{j,max}$ condition, we have $\dot{s}(x) \cdot s(x) < 0$. In conclusion, the control system based on the defined sliding manifold enforces the states of the system to reach the manifold intersection. By considering the convergence conditions, more than three droop gains can be implemented, as shown in Fig. 7. The possible paths of droop gain are illustrated by bold red and blue lines (e.g., D_3 *to* D_2 *or* D_3 *to* D_4).

Then, the bode plot describing the bang-bang loop function (Fig. 6) is illustrated in Fig. 8(a). As droop gain increases, the magnitude of function increase and also indicates that the phase angel delay becomes smaller when T decreases.

Furthermore, STATCOM is represented by the VSC model. In general, the IEEE committee uses short-circuit ratio (SCR) to describe grid strength for stability analysis of VSCs and defines a weak grid as SCR < 3 [36]. Several authors have already proved that the interaction between the current controller and phase-locked loop plays a significant role in provoking such unstable mechanisms [37], and the results show that a high droop gain makes the system less stable, with instability occurring at certain droop ranges. As shown in Fig. 8(b), the system was stable within certain droop gain ranges ($D < 29.2$), and a larger gain would make the system unstable. Thus, the stable droop range is predefined based on the droop stability analysis; see [37], [38] for results of related works.

B. Operation Strategy of Hybrid STATCOM

1) STATCOM Operation Strategy: In the typical fixed droop characteristic of STATCOM, STATCOM works in a capacitive mode when the voltage is lower than the reference voltage, and the STATCOM works in an inductive mode when the voltage is higher than the reference voltage. In the proposed adaptive droop control strategy, the defined dead-band facilitates the STATCOM to limit control action in the normal situations where the CBs or other reactive power resources keep working. STATCOMs are generally used in cases involving severe voltage fluctuations and/or voltage violations. The said cases include contingency and voltage fluctuations with immediate IBR power output. Because of the dead-band, the inter-oscillations can be reduced in the defined voltage range. At the same time, the STATCOM can independently choose two types of maximum and minimum capacitive droop slopes by estimating the adjacent reactive power recourse level for flexible STATCOM operation, as shown by red and blue traces in Fig. 5.

2) CB Operation Strategy: The CBs that are electrically close to the STATCOM or installed in the hybrid STATCOM systems have their own coordination scheme with the STATCOM to move the initial operation point to the maximum inductive region in the normal state. CBs are generally activated for steady-state voltage regulation such as an on-load tap changer. However, adopting the proposed adaptive droop scheme requires additional control logic as follows: 1) Measurement of the hybrid STATCOM system can show the POC voltage, available CB list, and current operation point of the STATCOM; 2) If the POC voltage is within the dead band, the x^{th} CB that satisfies the expression $min|Q_{j,L,max} - Q_j(t) - \sum_{x=1}^{l} Q_{CBs,x}(t)|$ is turned on. $Q_j(t)$ is the current reactive power output of the STATCOM, and $\sum_{x=1}^{l} Q_{CB,x}(t)$ is the currently available total reactive power amount of the CBs. Because of the action of the CBs, the STATCOM can have the maximum reactive power in capacitive mode. In conclusion, the proposed operation strategy of the hybrid STATCOM system is divided into three steps, as shown in Fig. 9.

VI. Case Studies

A. IEEE 39-Bus Standard Test System

To clearly show the simplicity and efficiency of the proposed adaptive control scheme using hybrid STATCOM with two IBR penetration levels, the IEEE 39-bus standard system was implemented, as shown in Fig. 10. The modified IEEE 39-bus standard system has 39 buses and 28 branches as it is, and the load bus follows an original busload value. However, the IBR and hybrid STATCOM system were newly attached at the 1, 4, 6, 21, 23, and 25 buses and the 5 and 22 buses, respectively. Buses 5 and 22 were selected for the following reasons:

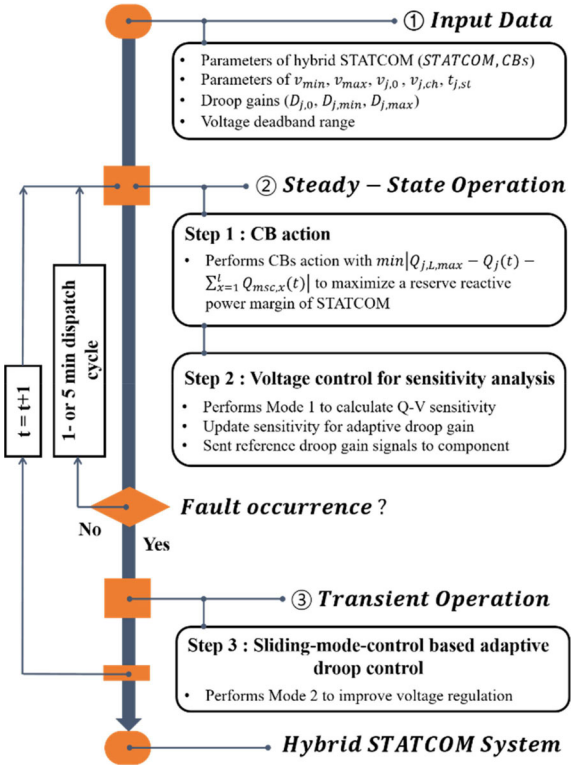

Fig. 9. Three-step workflow of adaptive droop control strategy of hybrid STATCOM.

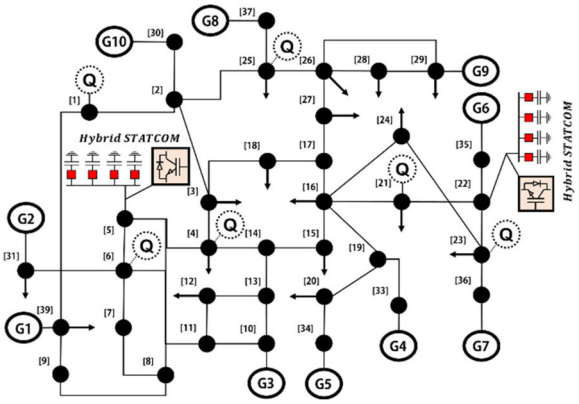

Fig. 10. Modified IEEE 39-bus standard test system.

- The STATCOM should not be attached near the conventional generators because they are operated in P–V control mode, which can show over-excitation and interference.
- The under-voltage problem at bus 5 and 22 is exhibited by calculating the power flow based on the amount of IBR generation.

The control parameters for STATCOM were as provided in Table II, and for STATCOM modeling, the PWM switching delay was then approximated by a first-order Padé approximation. Furthermore, the total reactive capacity and the location of the IBR and the hybrid STATCOM in the IEEE 39-test system were as shown in Tables III and IV.

TABLE II
STATCOM CONTROL PARAMETERS

PLL gain	120	V_{ch}	0.01 pu
PLL integral	1400	Nominal droop, D_0	0.03
k_{p1}	2	Converter Impedance, L	0.015 H
k_{p2}	2	Switch, S	0 or 1
k_{i1}	150	q-axis current control gain	1.5
k_{i2}	200	q-axis current control time constant	0.05

TABLE III
TOTAL REACTIVE POWER CAPACITY OF IBR

Bus	Capacity
1, 4, 6, 21, 23, and 25	±10 Mvar

TABLE IV
TOTAL REACTIVE POWER CAPACITY OF HYBRID STATCOM

index	CBs capacity (Mvar)	STATCOM capacity (Mvar)	
1	3	Capacitive	Inductive
2	5	20	10
3	5		
4	10		

TABLE V
AVAILABLE REACTIVE POWER OF STATCOM BY CBS ACTION

	Fixed droop	Adaptive droop
Capacitive	20 Mvar	40 Mvar

Because of the steady-state CB action, the STATCOM can attain the maximum reactive power in capacitive mode as shown in Table V. The initial operating point for the STATCOM is $Q \cong 0$ Mvar; thus, the available x^{th} CB was turned on to satisfy the expression $min|20\text{ Mvar} - 0\text{ Mvar} - \sum_{x=1}^{4} Q_{CB,x}|$. Hence, the 2nd, 3rd, and 4th CBs were turned on, and STATCOM had a maximum capacitive capacity of 40 Mvar, as shown in Table V.

B. Voltage-Sensitivity-Analysis Example in Mode 1

The example for sensitivity analysis operation for STATCOM is illustrated in this section. To measure $\partial Q/\partial v$, voltage regulation for STATCOM was performed by (9), and v_0 and v_{ch} were set as 1.039 pu and 0.006 pu, respectively. Hence, the voltage reference was continuously changed by 1.045 pu or 1.039 pu. The allowable POC voltage range is 0.95 pu to 1.05 pu, i.e., there is no over/under voltage violation and the sensitivity analysis can be operated within the deadband. In addition, the variation of v_{ch} is so small that there will be little impact on CB action or mutual interference with other reactive power sources.

Note that $\partial Q/\partial v$ was measured at 4.0-s intervals as an example. However, mode-1 operation should be activated at 1- or 5-min intervals during actual STATCOM operation. The sensitivity was predominantly affected by both total generation capacity and nearby reactive power resources; thus, measuring $\partial Q/\partial v$ at every economic dispatch cycle is reasonable.

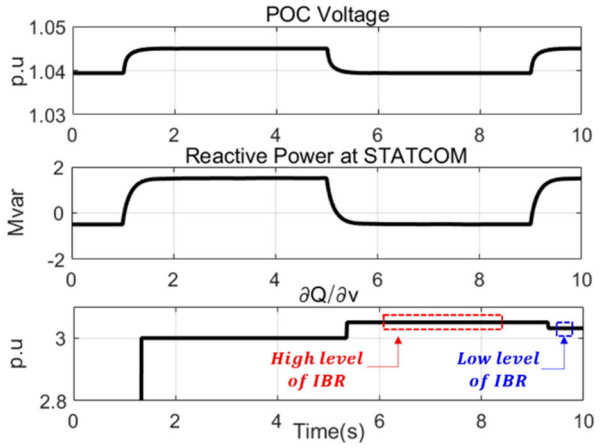

Fig. 11. Voltage sensitivity analysis mode: (a) POC voltage; (b) total reactive power of STATCOM; (c) $\partial Q/0.006$.

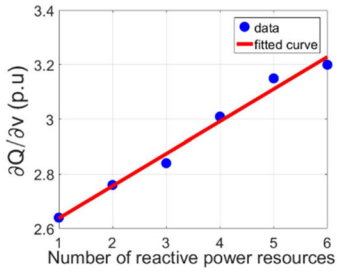

Fig. 12. Correlation between $\partial Q/\partial v_{ref}$ and IBR level ($v_{ch} = 0.05\ pu$).

The initial $\partial Q/\partial v$ was zero because there is no voltage reference change in STATCOM until $t = 1.3$ s as shown in Fig. 11(c). Next, the $\partial Q/\partial v$ was increased from 3 to 3.05 at $t = 5.3$ s because the high penetration level of IBR that tightly regulates its voltage was deliberately introduced. A large number of IBRs located next to the STATCOM hold their POC voltage; thus, a large total reactive current was used for regulating voltage. $\partial Q/\partial v$ was maintained until $t = 9.3$ s because there was no voltage reference change at STATCOM. By introducing two less IBRs into the grid, the $\partial Q/\partial v_{ref}$ was slightly decreased from 3.05 to 3.011 after $t = 9.3$ s because nearby IBRs were intentionally blocked from the grid. The correlation between $\partial Q/\partial v$ and IBR level is linear, as shown in Fig. 12.

Both $\partial Q_{min}/\partial v$ and $\partial Q_{max}/\partial v$ were also calculated based on $v_{ref} = 0.95$ pu and 1.05 pu by (9) based on the Korean power system grid code. Thus, it is anticipated that the interval between $\partial Q_{min}/\partial v$ and $\partial Q_{max}/\partial v$ at the j^{th} STATCOM is dependent upon the network topology.

C. Validation of the Proposed Adaptive Droop Scheme

The performance of the proposed scheme was validated in the following droop parameters in Table VI. The nominal droop gain D_0, the minimum droop gain D_{min}, and the maximum droop gain D_{max} were determined as 0.03, 0.01 and 0.1, respectively. As shown in Table VII, four scenarios were established based on two different levels of IBR. The fixed droop scheme adopts the nominal droop gain, whereas the adaptive droop strategy further applied two types of droop gains for all scenarios. It was assumed that IBR was operated based on the fixed Q–V droop by IEEE 1547 in cases 1, 2, and 4, and the reactive power sharing droop method was implemented in case 3. The comparison was based on the total reactive power output of the STATCOM at the buses 5, 22 and the IBR at bus 6 required by the voltage drop to observe the inter-converter interaction and the voltage regulation capability.

TABLE VI
DROOP GAIN RANGE FOR STATCOM

	D_0	D_{min}	D_{max}
Droop gain	0.03	0.01	0.1

TABLE VII
FOUR TYPES OF SCENARIOS AND DROOP GAINS

Case	IBR Bus	STATCOM Bus	$\partial Q/\partial v$	IBR droop gain (p.u)	STATCOM droop gain (p.u)
1	4, 6	5	2.9	0.03	0.03→0.01
2	1, 4, 6, 21, 23, 25	5	3.04	0.03	0.03→0.1→0.01
3	4, 6	5	2.9	0.15, 0.2	0.03→0.01
4	1, 4, 6, 21, 23, 25	5, 22	3.07	0.03	0.03→0.1→0.01

1) CASE 1 – Low IBR Level: The contingency timelines are as follows: 1) simulation start: 0 s, 2) apply 3-phase fault at bus 2: 1 s, 3) remove fault and trip lines: 1.083 s, and 4) simulation end: 4.0 s. For a low proportion of IBR in scenario 1 operating in the fixed droop scheme, the total reactive power was easily restricted, thereby limiting the capability of the IBR as compared to the case where the proportion of IBR was relatively high. According to Fig. 13(b), the reactive power of an IBR has a limited inverter capacity of ±10 Mvar; thus, the reactive power was frequently constrained at $t = 1.85$ s to 2.45 s. The fixed droop gain $D_0 = 0.03$ limits the additional large reactive output of the STATCOM; thus, the voltage profile with fixed droop is more unstable than that with an adaptive droop scheme, as shown by the red traces in Fig. 13(a), because of a shortage of reactive power and interference with the IBR. These results were compared, and it was found that a low proportion of IBRs need a low droop gain from the STATCOM. Using the fixed droop gain, the STATCOM contributed most to the incorrect compensation amount because the penetration level of the IBR was not considered.

In contrast, STATCOM with the adaptive droop scheme had the largest reserve reactive power as shown in Table V because the CBs were already actively involved before the contingency. Thus, the minimum voltage point was also improved, and inter-converter oscillations were mitigated, as shown by the blue trace in Fig. 13(a). The STATCOM estimates the adjacent IBR's level using the $\partial Q/\partial v$ results, indicating that the droop gain was decreased from $D' = 0.03$ to 0.01 to operate more sensitively at

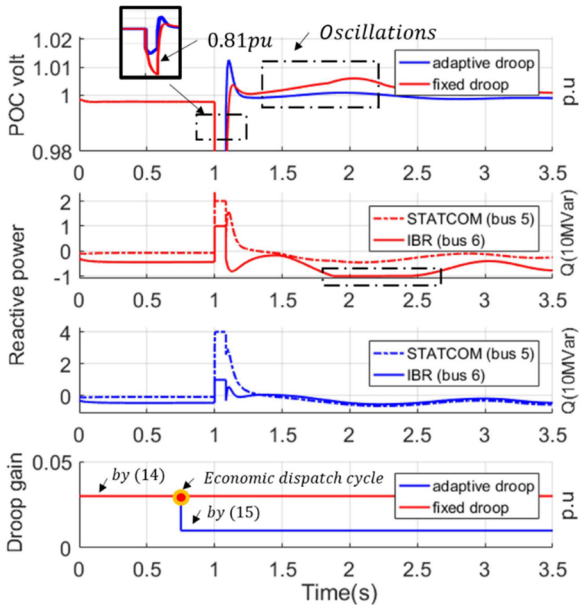

Fig. 13. Scenario 1: (a) voltage at bus 5; (b) reactive power output using fixed droop; (c) reactive power output using adaptive droop; (d) droop value.

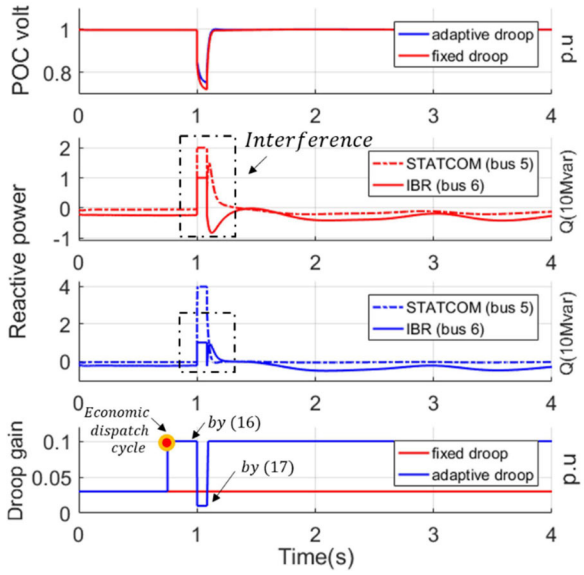

Fig. 14. Scenario 2: (a) voltage at bus 5; (b) reactive power output using fixed droop; (c) reactive power output using adaptive droop; (d) droop value.

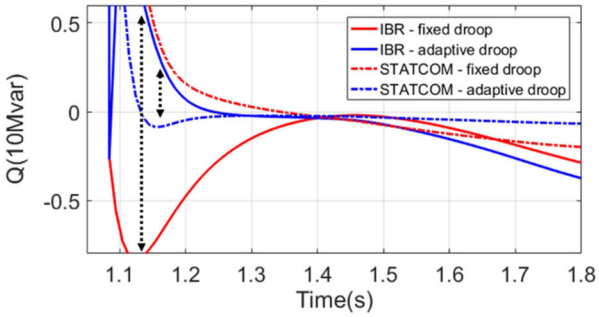

Fig. 15. Detailed inter-converter-oscillation results between adaptive and fixed droop schemes.

online economic dispatch time. At the same time, D' was set to 0.01 during a fault for a rapid dynamic response based on (17). Therefore, the STATCOM generated a maximum reactive power quickly, thereby ensuring voltage regulation, as demonstrated by the blue dotted trace in Fig. 13(c). The first case shows a shortage of reactive power in the network because of a low penetration of reactive power resources. Therefore, it is expected that a low droop gain is required in an off-peak load condition.

2) CASE 2 – High IBR Level: Scenario 2 was much more applicable to the IEEE 39-bus test system. The contingency timeline is the same as the first case. Given the increased level of IBRs, $\partial Q/\partial v$ was in the range of 2.92–3.20 such that the STATCOM increased its droop gain from $D' = 0.03$ to 0.1 to operate with less sensitivity at $t = 0.75$ s. This ensured that the voltage regulation was sufficient via six types of reactive power resources (1, 4, 6, 21, 23, and 25 buses). After a fault, D' was set to 0.01 during a low voltage time interval from $t = 1.0$ s to 1.083 s for rapid dynamic support.

Notable results of this scenario involved the interference. As shown by the four traces in Fig. 14(b) and (c), the oscillations in the adaptive droop scheme were sufficiently more reduced than the fixed droop gain during the time interval $t = 1.0$ s to 2.0 s because STATCOM was not actively involved in the voltage regulation. This control action also can conserve the reactive power while preparing for the *N*-1-1 contingency.

This is further substantiated by the reactive power output as shown in Fig. 15, which exhibits the inter-oscillation results in detail. The total area for degraded control action with red and blue lines depicts that the adaptive droop control achieved approximately two times better reactive power regulation than the fixed droop scheme. As represented by the two red lines at $t = 1.1$ s to 1.4 s, the two controllers inject or absorb reactive power because of different control modes and parameters. Notably, the sum of the two reactive powers converges to almost zero up until $t = 1.4$ s; some of the reactive current is unnecessarily wasted. To reduce the interference between controllers, time-delay settings or parameter adjustments are required. The former method requires a new time-delay setting procedure when a new IBR is connected to the grid; thus, the adaptive droop gain should be applied. As shown by the blue dotted trace in Fig. 15, reactive power generation was limited from the STATCOM, and it reduced its reactive power to almost zero via the proposed reactive power management.

3) CASE 3 – N-1-1 Contingency without CBs operation: To escalate the effectiveness of the proposed strategy, *N-1-1* contingency simulation without CB operation is performed. The voltage deviations from the nominal values due to the proposed droop algorithm depend on various factors including load impedance, number of IBRs connected to the grid, and the droop gains used. Therefore, it was assumed that the IBRs use all different droop gains based on the reactive power sharing method [39]. The power sharing method determines the reactive power demand from the IBRs and applies them for any combination of droop gains, irrespective of whether the inverters have identical droop gains. Therefore, it was assumed that the IBRs transmit the value of their respective reactive power output to the grid

and to the central controller by EMS. This reactive power value is broadcast to all the IBRs and each inverter determines the respective reactive power demand by dividing the received value with its droop gain. The droop gain can be determined by $D_x = Q_{total}/(Q_x^* \sum_{i=1}^{k} 1/D_i)$. Q_{total} is the reactive power supplied by all the inverters in network. Q_x^* is the reactive power demand for inverter x and D_x is the droop gain of inverter x.

To analyze the effects of reactive power sharing, droop gain is designed to share the reactive power between the IBRs. When there is a low proportion of IBR, the total number of IBRs is two and they have +20 Mvar. It was assumed that the reactive power demand for the first IBR is 8 Mvar, and droop gain of the first IBR can be calculated by $D_1 = 0.15$, and D_2 for 0.2. Using each droop gain of IBR, the fixed droop scheme and adaptive droop scheme were compared, and the contingency timelines were modified as follows: 1) simulation start: 0 s, 2) apply 3-phase fault at bus 2: 1 s, 3) remove fault and trip lines: 1.083 s, 4) apply 3-phase fault at bus 13: 1.135 s, 5) remove fault and trip lines: 1.2183 s, simulation end: 4.0 s.

The level of adjacent IBRs using $\partial Q/\partial v$ results indicate that the droop gain was decreased from $D' = 0.03$ to 0.01 to operate more sensitively at the online economic dispatch time. By not considering the network topology change, the droop gain is not changed in the fixed droop scheme.

The first notable results of this scenario involved the minimum voltage point. As can be seen, the minimum voltage of the fixed droop is similar to the adaptive droop scheme because under this case, the two strategies without CB actions will have the same amount of reserve reactive power in STATCOM. However, the voltage profile with the fixed droop is more unstable than that with an adaptive droop scheme, as can be verified using a high droop gain in primary control under low level of IBRs, as shown by the red trace in Fig. 16(a). This is further substantiated by the *N*-1-1 contingency. The blue traces in Fig. 16(b) show that the STATCOM provides higher reactive power at $t = 1.0$ s to 1.56 s.

The performance of the system when the proposed adaptive controller is enabled under reactive power sharing scheme of IBRs is validated in this case. As can be seen in Fig. 16(c), the droop gains of IBR at buses 4 and 6 are not identical, so the waveform of two reactive power output is different, in particular at $t = 1.2$ s to 2.5 s. Most importantly, the adaptive control of STATCOM does not affect the power sharing strategy. It is worth mentioning that if the adaptive gain is combined with the reactive power sharing of IBRs, more effective reactive power management can be obtained, especially under primary control. However, this implicitly assumes that all IBRs can be controllable, and therefore, not relies on conflicting goals. Moreover, the reactive power sharing method requires EMS to transmit the value of their respective reactive power output [39] so that the decentralized control cannot be achieved.

4) CASE 4 – N-1-1 Contingency with two hybrid STATCOMs: Additional tests were performed to verify the effect of the number of STATCOMs on voltage stability. In this case, one more hybrid STATCOM system using adaptive droop control scheme was considered to validate the performance of the proposed control strategy. Additional STATCOM is attached at bus 22

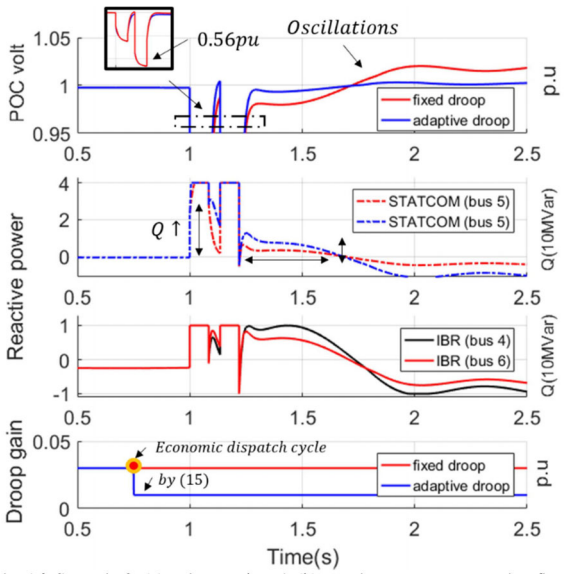

Fig. 16. Scenario 3: (a) voltage at bus 5; (b) reactive power output using fixed droop and adaptive droop under reactive power sharing strategy of IBRs; (c) reactive power output of IBRs under different droop gains; (d) STATCOM droop value.

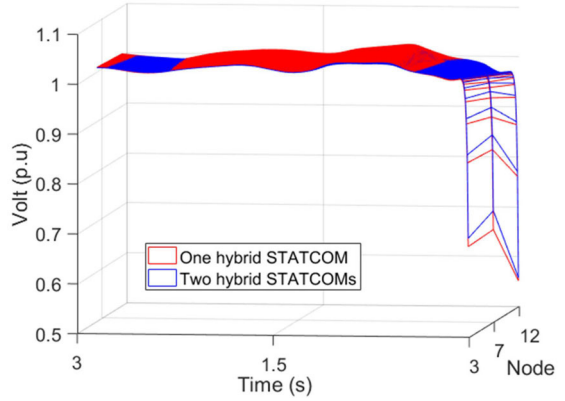

Fig. 17. Scenario 4: voltage recovery characteristic of at bus 3, 7 and 12.

to inject the reactive power to the right area of the test system in Fig. 10. Thus, two hybrid STATCOM systems were operated without EMS or other communication architectures.

As can be seen in Fig. 17, the voltage of the left side of the test system was restored to the nominal value in a similar waveform because the STATCOM at bus 5 already controlled the voltage with the adaptive droop scheme. In contrast, the STATCOM at bus 22 starts acting, which has more effect on the transients in comparison with the case when the one STATCOM is activated, as shown in Fig. 18. This is because the buses 16, 22, and 27 are located near the second hybrid STATCOM system.

As shown in Fig. 19, the minimum bus voltage points in the right area of the test system were also increased by about 0.1 pu, and the recovery profile was also improved, thereby indicating the effectiveness of the proposed adaptive droop control algorithm. Hence, the proposed algorithms achieve the requirements of decentralized control, voltage restoration according to the adjacent IBR's level considered

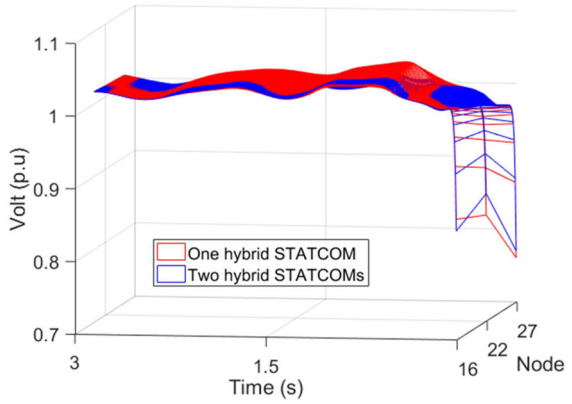

Fig. 18. Scenario 4: voltage recovery characteristic at bus 16, 22 and 27.

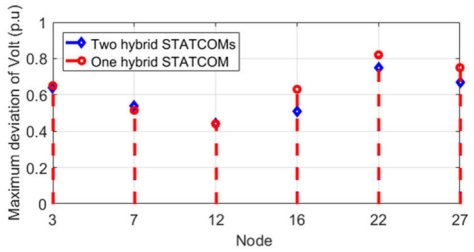

Fig. 19. Maximum voltage deviation between two cases.

and inverter-converter-oscillations, thereby indicating the effectiveness of the algorithm.

VII. Conclusion & Discussion

In this study, the sensitivity-analysis-based adaptive droop control strategy and the traditional fixed droop control with STATCOM were compared. This is particularly true with the use of multiple IBRs and the idea to apply adaptive droop has various advantages, as follows:

1) STATCOM can prepare for *N*-1-1 contingency and immediate IBR power output in the case of an uncertain penetration level of reactive power resources.
2) The proposed method is more useful than the earlier methods, which involve recalculation based on changing grid topologies.
3) It is easier to regulate the respective voltages without time delay settings.
4) Inter-converter oscillations can be relived.
5) STATCOM carries out decentral control automatically such that it eliminates the need for a central controller.
6) No knowledge of the network topology is required, and the architecture allows flexibility and redundancy.

As a future endeavor, the authors intend to address the coordinated control strategy between inverter-based reactive power resources and synchronous generators with fast and slow dynamics, respectively. The chattering issue of varying droop gain can be associated with exciter control of generators. Its effects on the overall damping at varying inverter and exciter parameter values will make for an interesting investigation.

References

[1] H. Gharavi and R. Ghafurian, *Smart Grid: The Electric Energy System of the Future*. Piscataway, NJ, USA: IEEE, 2011.
[2] P. P. Barker and R. W. De Mello, "Determining the impact of distributed generation on power systems. I. Radial distribution systems," in *Proc. Power Eng. Soc. Summer Meeting*, 2000, vol. 3, pp. 1645–1656.
[3] H. Shin, J. Jung, S. Oh, K. Hur, K. Iba, and B. Lee, "Evaluating the influence of momentary cessation mode in inverter-based distributed generators on power system transient stability," *IEEE Trans. Power Syst.*, vol. 35, no. 2, pp. 1618–1626, Mar. 2020.
[4] F. Nejabatkhah and Y. W. Li, "Overview of power management strategies of hybrid AC/DC microgrid," *IEEE Trans. Power Electron.*, vol. 30, no. 12, pp. 7072–7089, Dec. 2015.
[5] H. Su, P. Li, X. Fu, L. Yu, and C. Wang, "Augmented sensitivity estimation based voltage control strategy of active distribution networks with PMU measurement," *IEEE Access*, vol. 7, pp. 44987–44997, 2019.
[6] S. Song, S. Hwang, G. Jang, and M. Yoon, "Improved coordinated control strategy for hybrid STATCOM using required reactive power estimation method," *IEEE Access*, vol. 7, pp. 84506–84515, 2019.
[7] T. Basso, "IEEE 1547 and 2030 standards for distributed energy resources interconnection and interoperability with the electricity grid," Nat. Renewable Energy Lab., Golden, CO, USA, Tech. Rep.NREL/TP-5D00-63157, 2014.
[8] E. Ortjohann *et al.*, "A general architecture for modular smart inverters," in *Proc. IEEE Int. Symp. Ind. Electron.*, 2008, pp. 1525–1530.
[9] E. Ghiani and P. Fabrizio, "Smart inverter operation in distribution networks with high penetration of photovoltaic systems," *J. Modern Power Syst. Clean Energy*, vol. 3, no. 4, pp. 504–511, 2015.
[10] A. Kulmala, S. Repo, and P. Järventausta, "Coordinated voltage control in distribution networks including several distributed energy resources," *IEEE Trans. Smart Grid*, vol. 5, no. 4, pp. 2010–2020, Jul. 2014.
[11] G. C. Kryonidis, E. O. Kontis, A. I. Chrysochos, C. S. Demoulias, and G. K. Papagiannis, "A coordinated droop control strategy for overvoltage mitigation in active distribution networks," *IEEE Trans. Smart Grid*, vol. 9, no. 5, pp. 5260–5270, Sep. 2018.
[12] J. Momoh*et al.*, "Challenges to optimal power flow," *IEEE Trans. Power Syst.*, vol. 12, no. 1, pp. 444–455, Feb. 1997.
[13] J. Ansari, A. Gholami, and A. Kazemi, "Multi-agent systems for reactive power control in smart grids," *Int. J. Elect. Power Energy Syst.*, vol. 83, pp. 411–425, 2016.
[14] R. Aghatehrani and R. Kavasseri, "Sensitivity-analysis-based sliding mode control for voltage regulation in microgrids," *IEEE Trans. Sustain. Energy*, vol. 4, no. 1, pp. 50–57, Jan. 2013.
[15] J. M. Guerrero, M. Chandorkar, T.-L. Lee, and P. C. Loh, "Advanced control architectures for intelligent microgrids—Part I: Decentralized and hierarchical control," *IEEE Trans. Ind. Electron.*, vol. 60, no. 4, pp. 1254–1262, Apr. 2013.
[16] H. Liang, B. J. Choi, W. Zhuang, and X. Shen, "Stability enhancement of decentralized inverter control through wireless communications in microgrids," *IEEE Trans. Smart Grid*, vol. 4, no. 1, pp. 321–331, Mar. 2013.
[17] Z. Zhang, L. F. Ochoa, and G. Valverde, "A novel voltage sensitivity approach for the decentralized control of DG plants," *IEEE Trans. Power Syst.*, vol. 33, no. 2, pp. 1566–1576, Mar. 2018.
[18] G. Valverde and T. Van Cutsem, "Model predictive control of voltages in active distribution networks," *IEEE Trans. Smart Grid*, vol. 4, no. 4, pp. 2152–2161, Dec. 2013.
[19] H. Su, P. Li, X. Fu, L. Yu, and C. Wang, "Augmented sensitivity estimation based voltage control strategy of active distribution networks with PMU measurement," *IEEE Access*, vol. 7, pp. 44987–44997, 2019.
[20] L. Yu, D. Czarkowski, and F. De Leon, "Optimal distributed voltage regulation for secondary networks with DGs," *IEEE Trans. Smart Grid*, vol. 3, no. 2, pp. 959–967, Jun. 2012.
[21] M. E. Elkhatib, R. El-Shatshat, and M. M. Salama, "Novel coordinated voltage control for smart distribution networks with DG," *IEEE Trans. Smart Grid*, vol. 2, no. 4, pp. 598–605, Dec. 2011.
[22] T. Sansawatt, L. F. Ochoa, and G. P. Harrison, "Integrating distributed generation using decentralised voltage regulation," in *Proc. IEEE Power Energy Soc. General Meeting*, 2010, pp. 1–6.
[23] Y. Guo, Q. Wu, H. Gao, X. Chen, J. Østergaard, and H. Xin, "MPC-based coordinated voltage regulation for distribution networks with distributed generation and energy storage system," *IEEE Trans. Sustain. Energy*, vol. 10, no. 4, pp. 1731–1739, Oct. 2019.
[24] R. A. Jabr, "Robust volt/var control with photovoltaics," *IEEE Trans. Power Syst.*, vol. 34, no. 3, pp. 2401–2408, May 2019.

[25] Y. Lei, G. M. Burt, and S. Galloway, "Aggregated model of distribution networks with a large number of dispersed induction generators," in *Proc. Int. Conf. Sustain. Power Gener. Supply*, 2009, pp. 1–8.
[26] M. Khan, Y. Lin, B. Johnson, V. Purba, M. Sinha, and S. Dhople, "A reduced-order aggregated model for parallel inverter systems with virtual oscillator control," in *Proc. IEEE 19th Workshop Control Model. Power Electron.*, 2018, pp. 1–6.
[27] G. Reed*et al.*, "SDG&E Talega STATCOM project-system analysis, design, and configuration," in *Proc. IEEE/PES Transmiss. Distribution Conf. Exhib.*, 2002, vol. 2, pp. 1393–1398.
[28] E. John, A. Oskoui, and A. Petersson, "Using a STATCOM to retire urban generation," in *Proc. IEEE Power Energy Soc. Power Systems Conf. and Exposition*, 2004, 2004, pp. 693–698.
[29] Y. Ye, M. Kazerani, and V. H. Quintana, "Current-source converter based STATCOM: Modeling and control," *IEEE Trans. Power Del.*, vol. 20, no. 2, pp. 795–800, Apr. 2005.
[30] Y. Liu*et al.*, "Controller hardware-in-the-loop validation for a 10 MVA ETO-based STATCOM for wind farm application," in *Proc. IEEE Energy Convers. Congr. Expo.*, 2009, pp. 1398–1403.
[31] X. Fang, J. H. Chow, X. Jiang, B. Fardanesh, E. Uzunovic, and A.-A. Edris, "Sensitivity methods in the dispatch and siting of FACTS controllers," *IEEE Trans. Power Syst.*, vol. 24, no. 2, pp. 713–720, May 2009.
[32] A. Rahim, S. Al-Baiyat, and H. Al-Maghrabi, "Robust damping controller design for a static compensator," *IEE Proc.-Gener., Transmiss. Distribution*, vol. 149, no. 4, pp. 491–496, 2002.
[33] P. Kundur, N. J. Balu, and M. G. Lauby, *Power System Stability and Control*. New York, NY, USA: McGraw-hill 1994.
[34] J. W. Simpson-Porco, Q. Shafiee, F. Dörfler, J. C. Vasquez, J. M. Guerrero, and F. Bullo, "Secondary frequency and voltage control of islanded microgrids via distributed averaging," *IEEE Trans. Ind. Electron.*, vol. 62, no. 11, pp. 7025–7038, Nov. 2015.
[35] A. Yogarathinam and N. R. Chaudhuri, "Stability-constrained adaptive droop for power sharing in AC-MTDC grids," *IEEE Trans. Power Syst.*, vol. 34, no. 3, pp. 1955–1965, May 2019.
[36] Y. Huang, X. Yuan, J. Hu, and P. Zhou, "Modeling of VSC connected to weak grid for stability analysis of DC-link voltage control," *IEEE J. Emerg. Sel. Topics Power Electron.*, vol. 3, no. 4, pp. 1193–1204, Dec. 2015.
[37] Y. Huang and D. Wang, "Effect of control-loops interactions on power stability limits of VSC integrated to AC system," *IEEE Trans. Power Del.*, vol. 33, no. 1, pp. 301–310, Feb. 2018.
[38] C. Li, R. Burgos, B. Wen, Y. Tang, and D. Boroyevich, "Analysis of STATCOM small-signal impedance in the synchronous DQ frame." *IEEE J. Emerg. Sel. Topics Power Electron.*, vol. 8, no. 2, pp. 1894–1910, Jun. 2020.
[39] A. Micallef, M. Apap, C. Spiteri-Staines, J. M. Guerrero, and J. C. Vasquez, "Reactive power sharing and voltage harmonic distortion compensation of droop controlled single phase islanded microgrids," *IEEE Trans. Smart Grid*, vol. 5, no. 3, pp. 1149–1158, May 2014.

Sungyoon Song received the B.S degree in electrical engineering from Soongsil University, Seoul, South Korea, in 2015 and unified M.S. and Ph.D. degree in electrical engineering from Korea University, Seoul, Korea, in 2020. He has contributed to a wide variety of researches on the VSC-HVDC, FACTS system design and dynamic control. His research interests include probability power flow calculation using Python script.

Changhee Han received the B.S and M.S degrees in electrical engineering from Korea University, Seoul, Korea, in 2015 and 2017, respectively, where he is currently working toward the Ph.D. degree. His research interests include DC application on power system and distribution system operation.

Gyu-Sub Lee received the B.S., and unified M.S. and Ph.D. degrees in electrical engineering from Seoul National University, Seoul, South Korea, in 2013, 2020, respectively. He is currently a Senior Researcher with Seoul National University Electric Power Research Institute (SEPRI), Seoul, South Korea. His research interests include control and operation of HVDC system.

Roy A. McCann received the B.S. and M.S. degrees in electrical engineering from the University of Illinois at Urbana–Champaign, Champaign, IL, USA, in 1990 and 1991, respectively, and the Ph.D. degree in electrical engineering from the University of Dayton, Dayton, OH, USA, in 2001. From 1991 to 1994 he was a Design Engineer with General Motors. From 1994 to 1998, he was a Senior Project Engineer with ITT Automotive. From 1998 to 2003, he was with Delphi Automotive, Saginaw, MI, USA. In 2003, he joined the Faculty of the University of Arkansas, Fayetteville, AR, USA, where he is currently a Professor with the Department of Electrical Engineering and the Director of the Power Systems Control Laboratory. He is an Inventor on 20 U.S. patents and has authored or coauthored more than 100 technical articles. His research interests include modeling and control of large-scale renewable energy systems, power electronics, and electrical machinery.

Gilsoo Jang received the B.S. and M.S. degrees from Korea University, Seoul, South Korea, and the Ph.D. degree from Iowa State University, Ames, IA, USA, in 1997. He was with the Electrical and Computer Engineering Department, Iowa State University, as a Visiting Scientist for one year, and as a Researcher with Korea Electric Power Research Institute for two years. He is currently a Professor with the School of Electrical Engineering, Korea University. His research interests include power system dynamics and control.